Barton Journal

A Mathematical Approach to Prion Misfolding

FULL-LENGTH ARTICLE

Morgan Cassell*, Ashley L. Bennett+, and Nicole L. Mazuroski+

School of Health Sciences, Barton College, Wilson, NC, USA

*Student author, +Faculty mentor

CITATION

Cassell, Morgan; Bennett, Ashley L.; & Mazuroski, Nicole L. (2026). A mathematical approach to prion misfolding. *Barton Journal, 1*(1), 47–71. https://bartonjournal.org/vol-1-no-1/2026-cat1-article-no-002

© 2026 Morgan Cassell, Ashley L. Bennett, and Nicole L. Mazuroski. This article is published under the terms of the http://creativecommons.org/licenses/by/4.0/ License, which permits use, distribution and reproduction in any medium, provided the original work is properly cited.

Abstract

Prion diseases are a rare form of infectious neurodegenerative disorders that can infect humans as well as other mammals and can also be transferred from mammals to humans. Currently, these prion diseases remain both fatal and untreatable. These serious prion diseases are ultimately caused by the transformation of the prion protein (PrP^{c}), which is natively expressed in the central nervous system of mammals, into an infectious isoform, PrP^{sc}. High resolution NMR and cryo EM structures of PrP^{c} and PrP^{sc} have revealed vast structural differences between the two isoforms despite having the same amino acid sequence. While much is known about the specific structural differences between the native and infectious PrP isoforms, almost nothing is understood about the initial misfolding events triggering the PrP^{c} to fold into the PrP^{sc} or the specific details of how a misfolded PrP^{sc} infectious isoform and trigger a non-infectious PrP^{c} into the infectious isoform. Here, we provide a mathematical framework for studying prion structures and folding with the goal of building a predictive model. Leveraging experimentally derived constraints we demonstrate a topology-based model that enables a dimensionality reduction of the coordinate space by projection onto the contact space, thus enabling more efficient analysis of the interacting residues and interactions driving the PrP^{c} misfolding to PrP^{sc}. Now that this framework is established, we will integrate with biophysical, structural, and machine learning analyses

to explore the cellular factors that act as predictors for triggering a prion protein misfolding event.

Keywords: prion diseases, protein misfolding, prion protein, neurodegenerative disorders, mathematical modeling, topology, dimensionality reduction, contact space analysis, structural biology

---

Introduction

Prion diseases are a class of transmissible neurodegenerative disorders affecting a wide range of mammalian species. Human-specific prion diseases include Creutzfeldt-Jakob Disease (CDJ), Kuru, or Fatal Familial Insomnia (FFI) and remain untreatable and fatal. Prion diseases result when a transmutation of PrP^{c}, which is natively expressed in neurological tissue in mammals, is transformed into the infectious isoform, PrP^{sc}. Aggregation of the prion misfold causes a rapid deterioration of the neuron expressing fibril chains of PrP^{sc} (Miranzadeh Mahabadi & Taghibiglou, 2020).

Much like a viral disease, PrP^{sc} ultimately spreads and infects other nervous tissue in the central nervous system (CNS) of any host mammal. Although both isoforms share identical primary amino acid sequences consisting of approximately 210 residues after post-translational processing, where the difference lies in secondary and tertiary structure, resulting in a distinct fold between the two isoforms. PrP^{c} adopts a globular fold containing three a-helices and two short β-sheets while PrP^{sc} adopts a β-sheet rich fibrillar architecture, typically forming parallel, in-register β-sheets (Kovač & Čurin Šerbec, 2022; Kraus et al., 2021; Wille & Requena, 2018). Structural studies have identified structural variability in the $\beta 2$–$a 2$ loop (residues 165- 175) and the $a 2$–$a 3$ interhelical interface (residues 185-209), regions that are implicated in the transition from PrP^{c} to PrP^{sc} (Kraus et al., 2021). These regions provide plausible candidates for residue pairs (i', j') that contribute to the distance discrepancies between corresponding residue pairs, which can be measured with contact graphs and their threshold proximities. Residue pairs that show the largest differences in the contact maps are potential candidates for driving the misfold and structural separation between PrP^{c} and PrP^{sc}.

Prion proteins can take on many variations with one example being 1FO7, which is a mutant fragment from residues 90-231 containing 60 total conformations calculated, 30 of which have been verified and submitted. The same is true for a mammalian vector such as the Syrian Hamster (*M. auratus*), which examines residues 90-231 and has 100 calculated structures, 25 of which confirm the overall structural conformation of 2 β-sheets and 3 a-helices with sequences binding the 5 main structures of the globular domain.

The precise mechanism of this structural transition remains incompletely understood. This paper integrates topological and distance-geometric analyses to reveal the mechanism(s) of PrP^{c} and its infectious isoform PrP^{sc}. Subsequent stereochemical and structural analysis is used to map mathematical findings to the protein structures and reveal the underlying residue interactions driving prion protein misfolding.

Mathematical Methodology

The primary aim is to demonstrate through proof that a transformation from PrP^{c} to PrP^{sc} is defined and then map the mathematical transformation onto the prion protein isoform structures. While the real-world infectivity of the PrP^{sc} protein misfold is known, much is left unknown about misfolding initiating and propagation mechanisms. Resolving these mechanisms of pathogenesis requires a fresh perspective. We provide a mathematical model of structural transformation for representative prion protein structures 1QLX and 6LNI in $\mathbb{R}^1$, $\mathbb{R}^2$, and $\mathbb{R}^3$ representing sequence, contacts, and coordinate space, respectively. Given that we need a concrete and strong initial base, we can break down the analysis into multiple categories of application.

Proof in $\mathbb{R}^1$

Axiom 1:

Let Σ denotate the 20-letter amino acid alphabet. Post-enzymatic trimming, a mature PrP consists of 210 amino acid sequences. Therefore the sequence space is defined as;

$$S = \Sigma^{210} \text{ where, } \Sigma^{210} = \{a_i \in \Sigma \mid (a_1, a_2, a_3, \dots, a_{210})\}.$$

In addition, there does exist some $s \in S$ which represents an ordered 210-residue sequence.

Axiom 2:

Let $J: S \to Y$ be an invariant and define a relation $\sim_J$ on S by:

$$s \sim_J t \Leftrightarrow J(s) = J(t)$$

Lemma 1: Invariant-Induced Relations is an Equivalence Relation.

Claim: For any function $J: S \to Y$, the relation $\sim_J$ is an equivalence relation on S.

Proof: Define the following terms:

i. Reflexivity: $\exists\, a$ such that, $a = a$
ii. Symmetry: $\exists\, a, b$ such that, $a = b$ & $b = a$
iii. Transitivity: $\exists\, a, b, c$ such that, $a = b$ and $b = c \Longrightarrow a = c$.

Projecting these terms onto the initial claim results in:

i. If $J(s) = J(s)$, then $s \sim_J s$
ii. If $J(s) = J(t)$, then $J(t) = J(s)$
iii. If $J(s) = J(t)$ and $J(t) = J(u)$, then $J(s) = J(u)$.

Which then implies $\sim_J$ is reflexive, symmetric, and transitive. ▌

Axiom 3:

Define the identity invariance as:

$$J_1 : S \to S, J_1(s) = s,$$

Then the relation will satisfy:

$$s \sim_{J_1} t \Leftrightarrow s = t.$$

Because the prion conversion from globular PrP^c to infectious isoform PrP^{sc} is solely a conformational change and not a sequence or residue change, we can establish that the sequence is preserved regardless of conformational change. So, if we take some sequence:

$$s_c, s_{sc} \in S$$

Then the mature sequence residues will exist as:

$$s_c = s_{sc}.$$

Theorem 1: PrP Sequence Indistinguishability

Claim: under the primary invariance J_1, PrP^c and PrP^{sc} lie on the same equivalence class $S/\sim_{J_1}$.

Since: $s_c = s_{sc}$ we can say:

$$J_1(s_c) = s_c = s_{sc} = J_1(s_{sc})$$

$$\Longrightarrow J_1(s_c) = J_1(s_{sc})$$

$$\Longrightarrow s_c \sim_{J_1} s_{sc}$$

$$\Longrightarrow [s_c]_{J_1} = [s_{sc}]_{J_1} \blacksquare$$

Corollary for Theorem 1: Failure of Sequence-Level Detection Must Exist

Claim: no invariant depending solely on primary sequence identity can distinguish PrP^c from PrP^{sc}.

Since: $s_c = s_{sc}$ we can use direct substitution to impose:

$$\Longrightarrow J(s_c) = J(s_{sc}).$$

Therefore, if every invariant is defined solely on a primary sequence PrP which is contained in the enzymatic trimmed chain Σ^{210}, then both PrP^c and PrP^{sc} are indistinguishable. This is further elaborated in the biological perspective in which the PrP parent chain can be expressed either as the infectious fibril misfold or the native globular protein. Thus:

$$(\mathrm{PrP^c} = \mathrm{PrP^{sc}}) \subset \mathbb{R}^1 \blacksquare$$

Because experimentally we know that a misfold occurs somewhere in the protein life cycle, we are going to assume that fact and proceed forward in a fashion that emphasizes mathematical perspective. The goal is to then prove the non-congruence of $\mathrm{PrP^c}$ and $\mathrm{PrP^{sc}}$ in $\mathbb{R}^2$ and $\mathbb{R}^3$. As shown above, the $\mathbb{R}^1$ sequence space is congruent in residue sequence, however the two isoforms are known to be non-congruent in conformation. As the conformational $\mathbb{R}^3$ space is better described experimentally than the $\mathbb{R}^2$ contact space, the proof in $\mathbb{R}^3$ will be written first to easily observe the difference in structural conformation. That difference or conformational change in structure will be more easily presented through contact maps in the $\mathbb{R}^2$ proof.

Proof in $\mathbb{R}^3$

Axiom 4: Index Set

Let I be a finite residue index set on which both coordinate models supply. Concretely, I is taken to be the intersection of the residue indices present in:

- $\mathrm{PrP^c}$, which exists as a globular C-terminal domain and has 3 a-Helices and a short β sheet
- $\mathrm{PrP^{sc}}$, presents parallel in-register intermolecular β-sheets

$$I = (C) \cap (Sc).$$

Defining I as the overlap avoids any non-trivial index matching assumptions beyond the correlation to coordinates and labeled residues.

Axiom 5: Projection Mapping

Fix a representative atom per residue then define the embeddings as:

$$Fc{:}I \to \mathbb{R}^3, Fsc{:}I \to \mathbb{R}^3$$

Where $Fc(i)$ and $Fsc(i)$ be the 3D coordinates of the mmCIF atoms for the common residues in 1QLX and 6LNI, representing $\mathrm{PrP^c}$ and $\mathrm{PrP^{sc}}$, respectively.

Axiom 6: Rigid Motion

A rigid motion in $\mathbb{R}^3$ specifically is a representative mapping in form:

$$g(x) = Rx + v, R \in O(3), v \in \mathbb{R}^3.$$

Where the matrix R belongs to the orthogonal group $O(3)$, defined as:

$$O(3) = \{\mathbb{R} \in \mathbb{R}^{3x3} \mid R^T R = I\}$$

The main advantage of orthogonal matrices is that they preserve Euclidean inner product and thus lengths and

pairwise distances. Consequently, any transformation of the form $g(x) = Rx + v$ where $R \in O(3)$ and $v \in \mathbb{R}^3$ is a Euclidean isometry of $\mathbb{R}^3$. Distance matrices are therefore invariant under such transformations.

Axiom 7: Euclidean Congruence

Define Fc and Fsc as congruent if there exists a rigid motion g such that:

$$Fsc(i) = g(Fc(i)),\ \forall\, i \in I$$

Axiom 8: Distance Matrix on an Embedding

For an embedding in the projection $F{:}I \to \mathbb{R}3$, define its distance matrix D_F such that:

$$D_F{:}I \times I \to \mathbb{R}_{\geq 0},\ D_F(i,j) = \|F(i) - F(j)\|.$$

Given the following axioms, we can begin to establish lemmas 2 and 3 which state claims that rigid motion preserves pairwise distance, which was previously assumed in axiom 7 as well as a contrapositive separation.

Lemma 2: Rigid Motion Preserves Pairwise Distance

Claim: if $Fsc = g(Fc)$ for a rigid motion g then:

$$D_{F_{sc}}(i,j) = D_{F_c}(i,j),\ \forall\, i,j \in I.$$

Proof: $\forall\, i,j \in I$:

$$D_{F_{sc}}(i,j) = \|Fsc(i) - Fsc(j)\| = \|g(Fsc(i)) - g(Fsc(j))\|.$$

Given axiom 7 we can establish $g(x) = Rx + v$ with $R \in O(3)$ such that:

$$\|g(a) - g(b)\| = \|R(a - b)\| = \|a - b\|.$$

Therefore:

$$D_{F_{sc}}(i,j) = \|Fsc(i) - Fsc(j)\| = \|(RFc(i) + v) - (RFc(j) + v)\| = \|R(Fc(i) - Fc(j))\| = \|Fc(i) - Fc(j)\| = D_{F_{sc}}(i,j)\ \blacksquare$$

Lemma 3: Contrapositive Separation

Claim: If there exists a pair $i,j \in I$ such that:

$$D_{F_{sc}}(i,j) \neq D_{F_c}(i,j),$$

then there is no rigid motion g where $Fsc = g(Fc)$.

Proof: If lemma 2 holds true that if rigid motion g exists with $Fsc = g(Fc)$, then all corresponding pairwise distances must agree:

$$D_{F_{sc}}(i,j) = D_{F_c}(i,j),\ \forall\, i,j \in I.$$

Which is the implicit contrapositive of lemma 2 and thus if even 1 pair of residues satisfies:

$$D_{F_{sc}}(i,j) \neq D_{F_c}(i,j)$$

Then the embeddings cannot be related by any rigid motion. Therefore, Fsc and Fc are not Euclidean-congruent. ▮

This, however, is not sufficient evidence alone to establish a loose non-congruence of Euclidean space structures; there must be a witnessed pair that either one structure has, but the other one does not.

Axiom 9: Supremum of Distance Matrixes

Define the discrepancy between the two embeddings by the following:

$$\Delta\infty(Fc, Fsc) = \max_{i,j \in I} |D_{F_c}(i,j) - D_{F_{sc}}(i,j)|.$$

Since I is a finite set, this maximum will exist. This quantity represents the largest pairwise distance disagreement between the two respective embeddings.

Theorem 2: $\mathbb{R}^3$ Non-Congruence Explicit

Claim: From experimental data we assume:

$$\Delta\infty(Fc, Fsc) > 0$$

Therefore, there exists no rigid motion:

$$g(x) = Rx + v, R \in O(3),$$

such that:

$$Fsc = g(Fc).$$

Proof: If the embeddings were Euclidean congruent, then by Lemma 2:

$$D_{F_{sc}}(i,j) = D_{F_c}(i,j), \ \forall\, i,j \in I$$

$$\Rightarrow \Delta\infty(Fc, Fsc) = 0.$$

This contradicts the experimentally derived assumption that $\Delta\infty(Fc, Fsc) > 0$ and thus implies that there exist no rigid motion mapping Fc to Fsc. ▮

We then need to construct a witnessed pair that exists as the set's maximum pair, so we then define:

$$(i', j') \in I \times I$$

Such that:

$$\Delta\infty(Fc, Fsc) = |D_{F_c}(i', j') - D_{F_{sc}}(i', j')|$$

This identifies residues whose specific spatial separation has the largest discrepancy between the two embeddings. Thus:

$$D_{F_c}(i', j') \neq D_{F_{sc}}(i', j'),$$

which confirms an explicit geometric witness of the non-congruence between PrP^c and PrP^{sc}. To further strengthen the above theories and lemmas we will construct a contact graph.

Axiom 10: Contact Graph by an Embedding

Let the function F be defined as the projection of I onto real space:

$$F{:}I \to \mathbb{R}^3$$

Where I is an embedding of a finite index set, as previously stated. This allows for any fixed threshold $\delta > 0$ to define the graph $G(F, \delta)$ with edge set $E(F, \delta)$ such that:

$$G(F, \delta) = (I, E(F, \delta)),$$

Where:

$$(i,j) \in E(F, \delta) \Leftrightarrow \|F(i) - F(j)\| \leq \delta \text{ and } |i - j| > 2.$$

Theorem 3: Separation of Contact Graphs

Claim: If:

$$\Delta\infty(Fc, Fsc) > 0,$$

then $\exists\, \delta > 0$, such that:

$$G(Fc, \delta) \neq G(Fsc, \delta).$$

Proof: Because we know from the experimental assumption:

$$\Delta\infty(Fc, Fsc) > 0,$$

then there exist a witnessed pair such that:

$$D_{F_c}(i', j') \neq D_{F_{sc}}(i', j').$$

So, without loss of generality, we can assume:

$$D_{F_c}(i', j') < D_{F_{sc}}(i', j').$$

We will choose a δ such that:

$$\delta = \frac{D_{Fc}(i\prime,j\prime)+D_{FSc}(i\prime,j\prime)}{2}.$$

This then implies the following transformations:

$$D_{Fc}(i',j') \leq \delta < D_{Fsc}(i',j')$$

$$\Rightarrow (i',j') \in E(Fc, \delta) \text{ and } \nexists (i',j') \in E(Fsc, \delta)$$

$$\therefore E(Fc, \delta) \neq E(Fsc, \delta)$$

$$\Rightarrow G(Fc, \delta) \neq G(Fsc, \delta). \blacksquare$$

This establishes that there exists at least one witnessed pair (i',j') that belongs to one edge set but not the other, which implies that the corresponding contact graphs are non-congruent. To further this idea if we take into account the findings of Miranzadeh Mahabadi & Taghibiglou (2020), then we can observe that conformational misfolds of $PrP^{c} \rightarrow PrP^{sc}$ lies within the β2-*a*2 loop region (residues 165–175), and the *a*2-*a*3 inter-helical interfaces (residues 185–200) of PrP^{c}.

Proof in $\mathbb{R}^2$

Axiom 11: Orthogonal Planar Projections

Retain the same embeddings from the proof in $\mathbb{R}^3$ and with the same embeddings allowing I to be a finite index set of the specific PrP parent chain sequence:

$$Fc, Fsc: I \rightarrow \mathbb{R}^3.$$

If we then define 3 standard orthogonal planar projections, such that for any orthogonal projection denoted O can be represented as:

$$Oxy(x, y, z) = (x, y), Oxz(x, y, z) = (x, z), Oyz(x, y, z) = (y, z).$$

This reduction of geometric space gives 3 possible geometric planes as a result of each $Oa,b: \mathbb{R}^3 \rightarrow \mathbb{R}^2$, which is a linear mapping of $\mathbb{R}^3 \rightarrow \mathbb{R}^2$ created by deleting a single coordinate.

Axiom 12: Distance Structure Under Planar Projection

We can further define this mapping such that for any planar projection $F:I \rightarrow \mathbb{R}^2$ we define the embedding as:

$$D_F(i,j) = \|F(i) - F(j)\|,$$

where the double brackets denote the Euclidean norm on $\mathbb{R}^2$, which is:

$$\|x\| = \sqrt{x_1^2 + x_2^2}, \in \mathbb{R}^2.$$

Additionally, we state that for $P \in \{Oxy, Oxz, Oyz\}$:

$$D^{F_C^P}(i,j) = \|P(Fc(i) - Fc(Fc))\|, D^{F_{Sc}^P}(i,j) = \|P(Fsc(i) - Fsc(j))\|.$$

Axiom 13: Threshold Contact Graph on Planar Projections

To define the threshold graph on this 2-dimensional plane, we need to show that there exists some $\delta > 0$ such that:

$$G(F, \delta) = (I, E(F, \delta)),$$

where some ordered pair $(i,j) \in I$ can be defined as:

$$(i,j) \subset E(F, \delta) \Leftrightarrow \|F(i) - F(j)\| \leq \delta \text{ and } |i - j| > 2.$$

Lemma 4: Projection Identities

Claim: let there exist some vector ω such that $\omega = (x, y, z) \in \mathbb{R}^3$, then we can show:

$$\|Oxy(\omega)\|^2 + \|Oxz(\omega)\|^2 + \|Oyz(\omega)\|^2 = 2\|\omega\|^2.$$

Proof: $\omega = (x, y, z)$, which implies the following cases:

$$Oxy(\omega) = (x, y), Oxz(\omega) = (x, z), Oyz(\omega) = (y, z)$$

$$\Longrightarrow \|Oxy(\omega)\|^2 = x^2 + y^2$$

$$\Longrightarrow \|Oxz(\omega)\|^2 = x^2 + z^2$$

$$\Longrightarrow \|Oyz(\omega)\|^2 = y^2 + z^2.$$

This then give us:

$$(x^2 + y^2) + (x^2 + z^2) + (y^2 + z^2)$$

$$\Longrightarrow 2x^2 + 2y^2 + 2z^2$$

$$\Longrightarrow 2(x^2 + y^2 + z^2)$$

The internal portion of this product can be identified as the Euclidean norm in $\mathbb{R}^3$, which brings us back to our original vector that was proposed so we can conclude that:

$$x^2 + y^2 + z^2 = \|\omega\|^2 \Longrightarrow 2(x^2 + y^2 + z^2) = 2\|\omega\|^2$$

$$\therefore \|Oxy(\omega)\|^2 + \|Oxz(\omega)\|^2 + \|Oyz(\omega)\|^2 = 2\|\omega\|^2 \blacksquare$$

Lemma 5: Imposed Witness to Projection Identities

Claim: using the same pair of witnessed points $(i', j') \in I$ such that the witnessed points must exist in one plane or the other, allowing us to say:

$$\|Fc(i') - Fc(j')\| \neq \|Fsc(i') - Fsc(j')\|$$

$$\Longrightarrow \exists P \in \{Oxy, Oxz, Oyz\} \text{ such that,}$$

$$D^{F_C^P}(i', j') \neq D^{F_{Sc}^P}(i', j').$$

Proof: denote vectors v and u such that:

$$v = Fc(i') - Fc(j'), \text{ and } u = Fsc(i') - Fsc(j').$$

Given the hypothesis, neither v nor u can equal each other so we state that both v and u are unique vectors to the specific witnessed pair (i', j') thus:

$$\|v\| \neq \|u\|.$$

To demonstrate this, we will assume a contradiction that all 3 projections give equal distances on the plane:

$$\|Oxy(v)\| = \|Oxy(u)\|, \|Oxz(v)\| = \|Oxz(u)\|, \|Oyz(v)\| = \|Oyz(u)\|.$$

Given lemma 4 we can then say:

$$\|Oxy(v)\|^2 + \|Oxz(v)\|^2 + \|Oyz(v)\|^2 = \|Oxy(u)\|^2 + \|Oxz(u)\|^2 + \|Oyz(u)\|^2$$

$$\Longrightarrow 2\|v\|^2 = 2\|u\|^2$$

$$\Longrightarrow \|v\| = \|u\|$$

Thus, we reach a contradiction, and this shows that at least one of the coordinate planar projections must satisfy that:

$$\|P(v)\| \neq \|P(u)\|$$

$$\Longrightarrow D^{F_C^P}(i', j') \neq D^{F_{Sc}^P}(i', j')$$

for some unique projection $P \in \{Oxy, Oxz, Oyz\}$.∎

Theorem 4: Separating Planar Groups

If there exist a witnessed pair $(i', j') \in I$ such that:

$$\|Fc(i') - Fc(j')\| \neq \|Fsc(i') - Fsc(j')\|, P \in \{Oxy, Oxz, Oyz\}$$

with a unique threshold $\delta > 0$ such that:

$$G(F_C^P, \partial) \neq G(F_{Sc}^P, \partial).$$

Proof: Induce lemma 5 and then choose one of the 3 unique planar projections P:

$$D^{F_C^P}(i', j') \neq D^{F_{Sc}^P}(i', j').$$

Without a loss of generality, we can assume:

$$D^{F_C^P}(i', j') < D^{F_{Sc}^P}(i', j').$$

We then take a ∂ by the midpoint threshold such that:

$$\partial = \frac{D_{F_C^P}(i\prime, j\prime) + D_{F_{Sc}^P}(i\prime, j\prime)}{2},$$

which gives the statement:

$$D^{F_C^P}(i', j') \leq \partial < D^{F_{Sc}^P}(i', j')$$

$$\Longrightarrow (i', j') \in E(F_C^P, \partial)$$

$$\Longrightarrow (i', j') \notin E(F_{Sc}^P, \partial).$$

This then allows us to establish that the edge sets are not equal:

$$E(F_C^P, \partial) \neq E(F_{Sc}^P, \partial)$$

$$\Longrightarrow G(F_C^P, \partial) \neq G(F_{Sc}^P, \partial) \blacksquare$$

With an established witnessed pair existing, we can say that on the $\mathbb{R}2$ plane, there is at least one pair of coordinate projections that preserves distance inequality, as well as the threshold for that planar distance inequality produces graph separation.

Application

To demonstrate a provable and direct contact graph inequality, we need to interpret the proof through the biological context from which it was derived. The solution NMR structure 1QLX contains the experimentally determined 3D coordinates for globular PrP^c (Bank, 1999) and, alternatively, the coordinates for misfolding amyloid fibril PrP^{sc} are deposited in the high-resolution (2.70 Å) cryogenic electron microscopy (cryo-EM) structure (Data, 2019). This amyloid structure is a parallel in-register intermolecular beta sheet stack or PIRIBS (Data, 2019; Zahn et al., 2000). Several hypotheses propose mechanisms for both the initiating structural change within a neuron and the propagation of the infectious isoform. Here, we apply our mathematical framework with hopes to provide evidence in support of one of the plausible mechanisms of misfolding and

infectivity. To do so we apply the previously derived theorems that explain $\mathbb{R}^2$ & $\mathbb{R}^3$.

Applied proof in $\mathbb{R}^1$

While the PrP^c and PrP^{sc} proteins have the same amino acid sequence, there are some differences in the experimentally determined coordinate structure because of the protein purification process. Specifically, the prion protein purification protocol used to determine the 1QLX structure has a 17 amino acid residue N-terminal tail and a thrombin cleavage site engineered in. This engineered N-terminal sequence in PrP^c structure results in a direct difference in the encoding between PrP^c and PrP^{sc} such that there exist 2 N-terminal residues in the beginning of the 1QLX sequence as well as an N-terminus residue and C-terminal residue on the 6LNI. To accommodate this artifactual sequence change, we limit our analysis to the shared set of residues. This reduces the core residue count from each chain of 210 on each respective protein down to 208. This then allows us to analyze the following sequence code for Major Prion Protein (MPP):

> KKRPKPGGWNTGGSRYPGQGSPGGNRYPPQGGGGWGQPHGGGWGQPHGGGWGQPHG
> GGWGQPHGGGWGQGGGTHSQWNKPSKPKTNMKHMAGAAAAGAVVGGLGGYMLGSA
> MSRPIIHFGSDYEDRYYRENMHRYPNQVYYRPMDEYSNQNNFVHDCVNITIKQHTVTTT
> TKGENFTETDVKMMERVVEQMCITQYERESQAYYQRGS

To simplify the MPP residue chain into a more chewable or easily represented object, we will simply use the sigma notation from the previous Proof in $\mathbb{R}^1$,

$$MPP = \Sigma^{208},$$

where we can then denote 6LNI and 1QLX proteins as a projected reduction of the MPP residues. Specifically, the initial G and S on 1QLX and the beginning M and ending S on 6LNI, which are the respective termini, are truncated, such that we can denote 1QLX as C for a representation of PrP^c and 6LNI as Sc for PrP^{sc}:

$$C: \Sigma^{210} \to \Sigma^{208},\ C = \{a_3, a_4, a_5, \ldots, a_{208}, a_{209}, a_{210}\}$$

$$Sc: \Sigma^{210} \to \Sigma^{208},\ Sc = \{a_2, a_3, a_4, \ldots, a_{207}, a_{208}, a_{209}\}$$

This sequence only representation of MPP, which allows us to take the initial claim of $C = Sc$. Since both sequence representations are now equal to MPP, we can use MP to represent MPP such that the following is true:

$$MP = C = Sc \in \Sigma^{208}$$

We can then impose the identity invariant such that:

$$J_1: \Sigma^{208} \to \Sigma^{208},\ J_1(s) = s$$

$$\Longrightarrow J_1(C) = C = Sc = J_1(Sc)$$

$$\Longrightarrow C \sim_{J_1} Sc$$

$$\Longrightarrow [C]_{J_1} = [Sc]_{J_1},$$

if and only if :

$$MP = C = Sc \in \Sigma^{208}.$$

It should be noted that, based on the raw sequence with no exception to internal residue and considering the termini:

$$C \neq Sc \in \Sigma^{208}. \blacksquare$$

Applied proof in $\mathbb{R}^3$

To demonstrate Euclidean graph invariance, we select the witnessed pair of residues 176 and 190 between the 3D space of 6LNI and 1QLX because these pairs of residues confer not only a local witness of $|i - j| > 2$ but also a non-local witness using some delta as an anchor point.

Axiom 4: Re-applied

Let the index set be defined as the intersection of the structure coordinates of the residue pair, such that:

$$I = (C) \cap (Sc).$$

Limitations in current experimental structural biology lead to missing residue density in experimental PrP structures. Therefore, PDB structure representing *C* and *Sc* are incomplete. The 1QLX structure representing the PrP^c structure is missing residues 21-124 and 229-230 and thus contains coordinates for only the fragment 125-228, which is roughly the 104-count residue of the globular domain. The same exists for 6LNI where the fibril core exists as residues 170-229. This gives the intersecting set of:

$$I = (C) \cap (Sc)$$

$$C = \{125,\dots, 228\}, Sc = \{170,\dots, 229\}$$

$$\Longrightarrow I = (C) \cap (Sc) = \{170,\dots, 228\}$$

$$\Longrightarrow I = |59| \blacksquare$$

We then apply the distance graph of any witnessed pair:

$$i,j \in I, |i - j| > 2,$$

in which the witnessed pair of residues *i*,*j* exist within this 59-residue set. To show that the witnessed pair on both graphs is not equal, we use the residues 176 and 190 as the non-local witness such that $(i',j') = (176, 190)$. This allows us to determine:

$$|176 - 190| = 14 > 2.$$

To show that the pair is a non-local witness, we must project the coordinates of the witnessed pair to the distance graph. As is standard for structural biology analysis, we select the alpha carbon (*a*-carbon) atoms after a structural alignment between 1QLX and 6LNI to represent each residue. For the PrP^{c} structure 1QLX:

- Residue 176 $\in (-10.486, -14.457, -1.843)$
- Residue 190 $\in (-0.774, 1.083, -0.983)$.

And for PrP^{sc} structure 6LNI:

- Residue 176 $\in$ (205.776, 211.731, 243.361)
- Residue 190 $\in$ (179.099, 234.532, 241.349).

To get the residue pair distance for the distance graph we use:

$$Df(i,j) = \sqrt{(x_i - x_j)^2 + (y_i - y_j)^2 + (z_i - z_j)^2}$$

$$\Longrightarrow D_{F_c}(176, 190) = \frac{\sqrt{10517317}}{125\sqrt{2}}$$

$$\Longrightarrow D_{F_c}(176, 190) = \frac{\sqrt{10517317}}{125\sqrt{2}} \approx 18.34541 \text{ Å}.$$

The standardized data structure for mmCIF atom coordinate files on the PDB enables us to use a Python implementation to automate extraction of distances between the atoms and therefore a more accurate Ångstrom (where Å equals 10^{-10}m or one 10 billionth of a meter and a carbon-to-carbon single bond is ~1.54Å) distance such that for 1QLX the distance projection is:

$$D_{F_c}(176, 190) = 18.347626004 \text{ Å}$$

To show that a graph invariance exists, we perform the same analysis for the PrPSc structure 6LNI:

$$D_{F_{sc}} 176, 190) = \sqrt{(205.776 - 179.099)^2 + (211.731 - 234.532)^2 + (243.361 - 241.349)^2}$$

$$\Longrightarrow D_{F_{sc}}(176, 190) = \frac{\sqrt{617798037}}{500\sqrt{2}} \approx 35.15104.$$

And with the same code implementation, we can observe the encoded distance exists as:

$$D_{F_{sc}}(176, 190) = 35.151046556 \text{ Å}$$

This result demonstrates that not only does the distance graph of the witnessed non-local pair not equal each other but also that the computed residue distances in PrP^{c} and PrP^{sc} do not equal each other. We can now say

that:

$$D_{F_{sc}}(176, 190) \neq D_{F_c}(176,190)$$

This shows that no rigid motion exists in the contact graph. To further prove the two embeddings are not equal we can take the midpoint $\delta > 0$, which was defined in the proof, and compute the midpoint threshold such that:

$$\delta = \frac{18.347626004 + 35.151046556}{2} = 26.749336280 \text{ Å}.$$

And if,

$$D_{F_c}(176, 190) \leq \delta < D_{F_{sc}}(176, 190),$$

then we can determine:

$$(176, 190) \in E(Fc, \delta) \text{ and } (176, 190) \notin E(Fsc, \delta)$$

$$\therefore G(Fc, \delta) \neq G(Fsc, \delta) \blacksquare$$

Using our implementation, we can automate this analysis over all combinations of residue pairs in the 59-residue intersection of the PrP^c and PrP^{sc} structures, building a network graph for all possible witnessed local and non-local residue pairs (Figure 1). This comprehensive network graph demonstrates clearly that the edge set and the connectivity between the edges differ between the PrP^c and PrP^{sc} structures. In the context of structural biology, this means that there are differences in the residues making up the edge sets and how the residues interact with each other in the two isoforms.

Figure 1

Network Graphs of PrP^c and PrP^{sc}

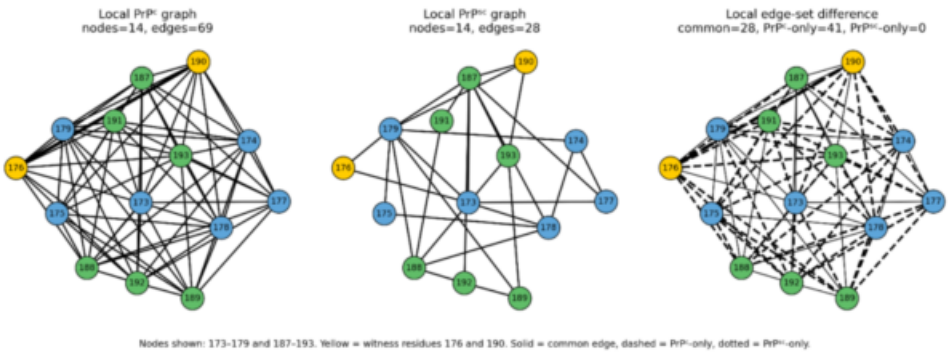

Note. Local network graphs for the intersecting residue set 173–179 and 187–193 in (*left*) PrP^c, (*middle*) PrP^{sc}, and (*right*) the difference between PrP^c and PrP^{sc}. The nodes represent the *a*-carbon atoms of the residues and the edges the interactions between residues in the PrP structures. Yellow (176,190) represents the witnessed

pair selected during the application of the proof. In the panel on the right showing the edge set differences, the solid lines show interactions in common between PrP^{c} and PrP^{sc}, while the dashed and dotted lines represent interactions that are present only in PrP^{c} or PrP^{sc}, respectively.

Applied proof in $\mathbb{R}^2$

To show that there exists a unique orthogonal projection, we impose the same *a*-carbon coordinates such that the difference between the unique witnessed pair (176, 190) would be:

$$F(176) - F(190) = (x_{176} - x_{190}, y_{176} - y_{190}, z_{176} - z_{190})$$

$$\Longrightarrow Fc(176) - Fc(190) = (-9.712, -15.540, -0.906) = C$$

$$\Longrightarrow Fsc(176) - Fsc(190) = (26.677, -22.801, 2.012) = Sc.$$

We can then reduce the dimensionality of the geometric space by constructing a projection from geometric space to relational contact map space, which was previously demonstrated. Given that $\mathbb{R}3$ proof remains true, we can say the previous difference remains true for all values of projection. We define the top value as C and the bottom value to Sc to simplify the projection results. To begin with the proof, all 3 orthogonal planar projections must be observed.

Projection to *xy*

The *xy* projection is shown in Figure 2 and calculated from:

$$Oxy(C) = (-9.712, -15.540), \text{ and } Oxy(Sc) = (26.677, -22.801)$$

$$\Longrightarrow D^{xy}_{F_C}(176, 190) = \|Oxy(C)\| = \sqrt{(-9.712)^2 + (-15.540)^2} = 18.325243354$$

$$\Longrightarrow D^{xy}_{F_{Sc}}(176, 190) = \|Oxy(Sc)\| = \sqrt{(26.677)^2 + (-22.801)^2} = 35.093417188$$

$$\Longrightarrow \partial xy = \frac{18.325243354 + 35.093417188}{2} = 26.709330271 \text{ Å}$$

$$\Longrightarrow D^{xy}_{F_C}(176, 190) \leq \partial xy < D^{xy}_{F_{Sc}}(176, 190)$$

$$\Longrightarrow (176,190) \in E(F_C^{xy}, \partial) \text{ and } (176, 190) \notin E(F_{Sc}^{xy}, \partial)$$

$$\Longrightarrow E(F_C^{xy}, \partial) \neq E(F_{Sc}^{xy}, \partial)$$

$$\therefore G(F_C^{xy}, \partial xy) \neq G(F_{Sc}^{xy}, \partial xy).$$

Figure 2

xy Projection

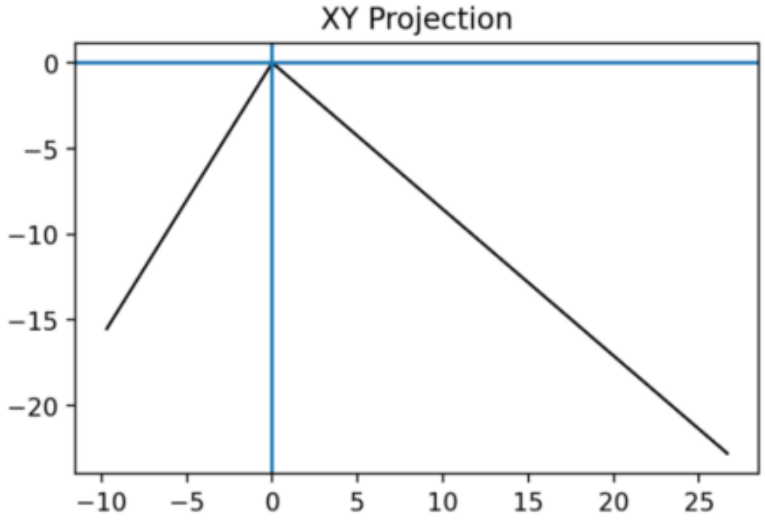

Note. The *xy* projection of the geometric space onto the relational contact space.

This first orthogonal planar projection already demonstrates that at least one projection exhibits a contact graph difference. However, to be as rigorous as possible, we continue the application with the remaining 2 projections.

Projection to *xz*

$$Oxz(C) = (-9.712, -0.906), \text{ and } Oxz(Sc) = (26.677, 2.012)$$

$$\Rightarrow D_{F_C}^{xz}(176,190) = \|Oxz(C)\| = \sqrt{(-9.712)^2 + (-0.906)^2} = 9.754167314$$

$$\Rightarrow D_{F_{Sc}}^{xz}(176, 190) = \|Oxz(Sc)\| = \sqrt{(26.677)^2 + (2.012)^2} = 26.752765707$$

$$\Rightarrow \partial xz = \frac{9.754167314 + 26.752765707}{2} = 18.25346651 \text{ Å}$$

$$\Rightarrow D_{F_C}^{xz}(176, 190) \leq \partial xz < D_{F_{Sc}}^{xz}(176, 190)$$

$$\Rightarrow (176,190) \in E(F_C^{xz}, \partial) \text{ and } (176, 190) \notin E(F_{Sc}^{xz}, \partial)$$

$$\Rightarrow E(F_C^{xz}, \partial) \neq E(F_{Sc}^{xz}, \partial)$$

$$\therefore G(F_C^{xz}, \partial xz) \neq G(F_{Sc}^{xz}, \partial xz).$$

Figure 3

xz Projection

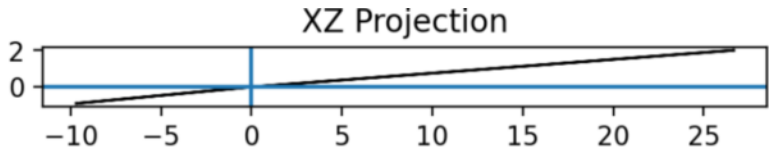

Note. The *xz* projection of the geometric space onto the relational contact space.

Thus, there exists now a second planar projection where a graph invariance is observed (Figure 3).

Projection to *yz*

$$Oyz\,(C) = (-15.540,-0.906), \text{ and } Oyz\,(Sc) = (-22.801,2.012)$$

$$\Longrightarrow D_{F_C}^{yz}\,(176, 190) = \|Oyz\,(C)\,\| = \sqrt{(-15.540)^2 + (-0.906)^2} = 15.566388$$

$$\Longrightarrow D_{F_{Sc}}^{yz}\,(176, 190) = \|Oyz\,(Sc)\| = \sqrt{(-22.801)^2 + (2.012)^2} = 22.8895991$$

$$\Longrightarrow \partial yz = \frac{15.566388 + 22.8895991}{2} = 19.22799355 \text{ Å}$$

$$\Longrightarrow D_{F_C}^{yz}\,(176, 190) \leq \partial yz < D_{F_{Sc}}^{yz}\,(176, 190)$$

$$\Longrightarrow (176,190) \in E(F_C^{yz}, \partial) \text{ and } (176, 190) \notin E(F_{Sc}^{yz}, \partial)$$

$$\Longrightarrow E(F_C^{yz}, \partial) \neq E(F_{Sc}^{yz}, \partial)$$

$$\therefore\ G(F_C^{yz}, \partial yz) \neq G(F_{Sc}^{yz}, \partial yz).$$

Figure 4

yz Projection

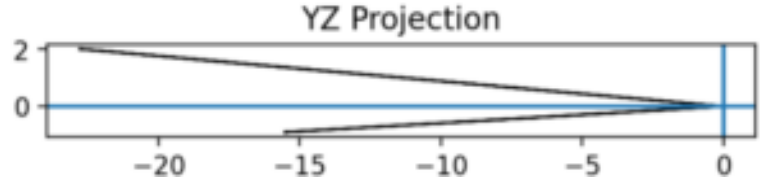

Note. The *yz* projection of the geometric space onto the relational contact space.

The three orthogonal planar projections (Figures 2–4) show that regardless of which chosen planar coordinates

of the witness pair (176, 190) that you will find a discrepancy between their embeddings. This further enforces the original claim of the structural conformation having vastly different structures.

Interpretation

We leverage several key implementations of metric space calculations in the $\mathbb{R}^1$, $\mathbb{R}^2$ and $\mathbb{R}^3$ proofs. Beginning with the initial proof in $\mathbb{R}1$, the concept was introduced of projecting a protein structure into its sequence-based representation. This framework relied on the assumption that both the infectious fibril and the non-infectious version of the major prion protein isoforms are simply expressions of PrP, and that neither protein was assumed to possess terminal edges within their globular domains. Due to the limitations of experimental structural biology methods and their inability to fully resolve atomic positions in flexible protein structures such as PrP, the applied proof in $\mathbb{R}^1$ required stripping the terminal residues of PrP^c and PrP^{sc} and using only purely the backbone of the residues representing the globular domain in the native PrP^c. This truncated sequence space representing the intersection of experimentally resolved residues was then shown to be equivariant using invariances. In other words, there was no way to tell the difference between MPP, *C*, *Sc* given solely their backbone sequence code. Because we cannot differentiate the isoforms in $\mathbb{R}^1$, we use the experimentally observable difference in structure as an assumption to show through proof in $\mathbb{R}^3$ that the structures are indeed different.

The proof in $\mathbb{R}^3$ was designed to show that each contact graph of the proteins had at least one delta which denoted a fixed midpoint for the edge sets to be derived from and allowed for a distance variance to be determined. This was further established in the applied proof where we use the 3D coordinates space from the mmCIF files to calculate the atom distances in PrP^c and PrP^{sc} (Table 1).

Table 1

Coordinates for Witnessed Non-Local Residue Pairs in PrPC and PrPSc

Structure	**Residue**	**X** (Å)	**Y**(Å)	**Z**(Å)
1QLX	176	-10.486	-14.457	-1.843
1QLX	190	-0.774	1.083	-0.937
6LNI	176	205.776	211.731	243.361

6LNI	190	179.09 9	234.53 2	241.3 49

Note. The 1QLX and 6LNI structures provide the coordinates for PrP^{c} and PrP^{sc}, respectively. The X, Y, and Z coordinates expressed in Ångstroms (Å) for the residues 176 and 190 composing the witnessed non-local residue pair in the application of proofs.

The coordinates of the witnessed non-local pair in both $PrP^{c}$and PrP^{sc} structures give the ability to determine through a Euclidean norm that there is a midpoint for the set of intersecting residues representing the native globular domain. We can then use this midpoint as the anchor for distance projection. The distance projection reveals key differences between the two proteins; specifically, when we examine the midpoint delta, only one protein isoform satisfies the projected inequality, such that witnessed pair (176,190) remains within the edge set for the PrP^{c} isoform.

To further demonstrate that there is a difference between the two isoforms, we use the $\mathbb{R}2$ proof to accomplish a projection that successfully reduces the dimensions of witnessed non-local residue pair and thus simplifies computations. We perform a reduction in dimensional space such that, when analyzing any two planar projections of a three-dimensional structure, we can establish that there will be at least one view within that spatial reduction that demonstrates the witnessed pair does not exist in either edge set, and therefore in neither graph projection. This incongruity in graph projections is confirmed for every 3D planar projection in $\mathbb{R}3$regardless of dimensional combination. This further strengthens the claim that there exists a conformational difference between PrP^{c} and PrP^{sc}.

Discussion

As this paper currently stands, there is very little addition to biochemistry, stereochemistry, biophysics, combinatorics, or ionic interaction theory. This will be addressed in the 'Further Research' portion of this paper. Currently, this is an analysis of the basest level that observes sequence variation and applied that onto a 3-dimensional structural space, and that allows for an ability to show a difference in physical properties. The addition of ionic interaction theories as well as proton channels that help regulate cell pH in the CNS is actively being considered as well as further structural analysis of the fibril that PrP^{sc} creates and signaling effects in the host neuron.

Conclusion

A key conclusion from this study is that the edge sets in the contact graphs do represent interacting partners, defined by the chosen distance thresholds between the witnessed residue pairs. However, the presence of an edge does not automatically imply a functional or causative interaction; for example, residues that are distant in the structure may or may not influence protein behavior through allosteric mechanisms, while more local contacts are likely to be more directly relevant. The observed differences in contact graphs reflect how these interactions

act as structural variables and are incrementally modified, rather than providing a direct mapping to ionic interaction theory, biophysical interactions, or conformational dynamics. Importantly, this model aligns with current physical observations that the two forms of the major prion protein, PrP^{c} and PrP^{sc}, are structurally distinct, despite having identical primary sequences.

Further Research

This paper presents findings from ongoing research conducted by Ashley L. Bennett, PhD, and Nicole L. Mazuroski, M.S. Moving forward, this study proposes to incorporate electrostatic and ionic interaction principles to better understand protein conformational dynamics. Specifically, it is hypothesized that metabolic stressors may induce a localized decrease in pH within the central nervous system, leading to an increased concentration of free hydrogen ions promoting protonation of key amino acid residues and inducing backbone conformational changes through altered salt bridge interactions. Additionally, interacting partners of PrP^{c}, may further modulate the local proton environment. For example, zinc may influence neuronal acidity by interfering with proton transport mechanisms, potentially reducing proton efflux, and contributing to intracellular proton accumulation. There is also ongoing discussion about the potential intracellular interactions of calcium, chloride, and copper, although these ideas remain speculative at this stage.

References

Anand, Uttam; Patra, Shubhadeep; Sekar, Rohith Vedhthaanth; Garen, Craig R.; & Woodside, Michael T. (2025). Different folding mechanisms in prion proteins from mammals with different disease susceptibility observed at the single-molecule level. *Proceedings of the National Academy of Sciences, 122*(29). https://doi.org/10.1073/pnas.2416191122

Andre, Ralph & Tabrizi, Sarah J. (2012). Misfolded PrP and a novel mechanism of proteasome inhibition. *Prion, 6*(1), 32–36. https://doi.org/10.4161/pri.6.1.18272

Artikis, Efrosini; Kraus, Allison; Caughey, Byron. (2022). Structural biology of ex vivo mammalian prions. *Journal of Biological Chemistry, 298*(8), 102181.https://doi.org/10.1016/j.jbc.2022.102181

Blumenthal, Leonard M. (1953). *Theory and applications of distance geometry* (1st ed.). Oxford at the Clarendon Press. https://archive.org/details/theoryapplicatio0000leon/page/n7/mode/2up

Boon Seng Wong; Liu, Tong; Li, Ruliang; Pan, Tao; Petersen, Robert B.; Smith, Mark A.; Gambetti, Pierluigi; Perry, George; Manson, Jean C.; Brown, David R.; Sy, Man Sun . (2001). Increased levels of oxidative stress markers detected in the brains of mice devoid of prion protein. *Journal of Neurochemistry, 76*(2), 565–572. https://doi.org/10.1046/j.1471-4159.2001.00028.x

Brown, David R. (2001). Copper and prion disease. *Brain Research Bulletin, 55*(2), 165–173. https://doi.org/10.1016/s0361-9230(01)00453-1

Brown, David R.; Qin, Kefeng; Herms, Jochen; Madlung, Axel; Manson, Jean; Strome, Robert; Fraser, Paul E.; Kruck, Theo; von Bohlen, Alex; Schulz-Schaeffer, Walter; Giese, Armin; Westaway, David; & Kretzschmar, Hans (1997). *The cellular prion protein binds copper in vivo. Nature, 390*(6661), 684–687. https://doi.org/10.1038/37783

Canoyra, Sara; Marín-Moreno, Alba; Espinosa, Juan Carlos; Fernández-Borges, Natalia; Vidal, Enric; Orge, Leonor; Benestad, Sylvie L.; Andréoletti, Olivier; & Torres, Juan María (2025). Classical BSE emergence from Nor98/atypical scrapie: Unraveling the shift vs. selection dichotomy in the prion field. *Proceedings of the National Academy of Sciences, 122*(29). https://doi.org/10.1073/pnas.2501104122

De La Rosa, Victor; Bennett, Ashley L.; & Ramsey, I. Scott. (2018). Coupling between an electrostatic network and the Zn2+ binding site modulates Hv1 activation. *The Journal of General Physiology, 150*(6), 863–881. https://doi.org/10.1085/jgp.201711822

Diestel, Reinhard. (2025). *Graph theory*. Springer.

Edgeworth, Julie Ann; Jackson, Graham S.; Clarke, Anthony R.; Weissmann, Charles; & Collinge, John. (2009). Highly sensitive, quantitative cell-based assay for prions adsorbed to solid surfaces. *Proceedings of the National Academy of Sciences, 106*(9), 3479–3483. https://doi.org/10.1073/pnas.0813342106

Gogte, Kalpshree; Mamashli, Fatemeh; Herrera, Maria Georgina; Kriegler, Simon; Bader, Verian; Kamps, Janine; Grover, Prerna; Winter, Roland; Winklhofer, Konstanze F.; & Tatzelt, Jörg. (2024). Topological confinement by a membrane anchor suppresses phase separation into protein aggregates: Implications for prion diseases. *Proceedings of the National Academy of Sciences, 122*(1). https://doi.org/10.1073/pnas.2415250121

Hirsch, Morris W. (1997). *Differential topology* (Corr. 6. print). Springer.

James, Thomas L.; Liu, He; Ulyanov, Nikolai B.; Farr-Jones, Shauna; Zhang, Hong; Donne, David G.; Kaneko, Kiyotoshi; Groth, Darlene; Mehlhorn, Ingrid; Prusiner, Stanley B.; & Cohen, Fred E. (1997). Solution structure of a 142-residue recombinant prion protein corresponding to the infectious fragment of the scrapie isoform. *Proceedings of the National Academy of Sciences, 94*(19), 10086–10091. https://doi.org/10.1073/pnas.94.19.10086

Matoušek, Jirí. (2002). *Lectures on discrete geometry*. Springer.

Kamali-Jamil, Razieh; Vázquez-Fernández, Ester; Tancowny, Brian; Rathod, Vineet; Amidian, Sara; Wang, Xiongyao; Tang, Xinli; Fang, Andrew; Senatore, Assunta; Hornemann, Simone; Dudas, Sandor; Aguzzi, Adriano; Young, Howard S.; & Wille, Holger. (2021). The ultrastructure of infectious L-type bovine spongiform encephalopathy prions constrains molecular models. *PLOS Pathogens, 17*(6), e1009628. https://doi.org/10.1371/journal.ppat.1009628

Kawauchi, Akio. (2011). Topology of prion proteins: A joint work with Kayo Yoshida. In *Special Session on Knotting in Linear and Ring Polymer Models* [Conference]. AMS Sectional Meeting. https://user.keio.ac.jp/~ishikawa/tms2011/files/tms2011_kawauchi.pdf

Kovač, Valerija; & Čurin Šerbec, Vladka (2022). Prion Protein: The Molecule of Many Forms and Faces. *International Journal of Molecular Sciences, 23*(3), 1232. https://doi.org/10.3390/ijms23031232

Kraus, Allison; Hoyt, Forrest; Schwartz, Cindi L.; Hansen, Bryan; Artikis, Efrosini; Hughson, Andrew; Raymond, Gregory J.; Race, Brent; Baron, Gerald S.; & Caughey, Byron. (2021). *High-resolution structure and strain comparison of infectious mammalian prions. Molecular Cell, 81*(21). https://doi.org/10.1016/j.molcel.2021.08.011

Lee, John M. (2013). *Introduction to smooth manifolds* (2. edition). Springer.

Masone, Antonio; Zucchelli, Chiara; Caruso, Enrico; Lavigna, Giada; Eraña, Hasier; Giachin, Gabriele; Tapella, Laura; Comerio, Liliana; Restelli, Elena; Raimondi, Ilaria; Elezgarai, Saioa R.; De Leo, Federica; Quilici, Giacomo; Taiarol, Lorenzo; Oldrati, Marvin; Lorenzo, Nuria L.; García-Martínez, Sandra; Cagnotto, Alfredo; Lucchetti, Jacopo; Gobbi, Marco; Vanni, Ilaria; Nonno, Romolo; Di Bari, Michele A.; Tully, Mark D.; Cecatiello, Valentina; Ciossani, Giuseppe; Pasqualato, Sebastiano; Van Anken, Eelco; Salmona, Mario; Castilla, Joaquín; Requena Requena; Banfi, Stefano; Musco, Giovanna; Chiesa, Roberto. (2023). A tetracationic porphyrin with dual anti-prion activity. *iScience, 26*(9), 107480. https://doi.org/10.1016/j.isci.2023.107480

De Berg, Mark; Cheong, Otfried; & Overmars, Mark. (2008). *Computational geometry: Algorithms and applications* (3rd ed). Springer.

Miranzadeh Mahabadi, H., Hajar & Taghibiglou, Changiz.(2020). Cellular Prion Protein (PrPc): Putative Interacting Partners and Consequences of the Interaction. *International Journal of Molecular Sciences, 21*(19), 7058. https://doi.org/10.3390/ijms21197058

Ruffin, Vernon A.; Salameh, Ahlam I.; Boron, Walter F.; & Parker, Mark D. (2014). Intracellular pH regulation by acid-base transporters in mammalian neurons. *Frontiers in Physiology, 5*. https://doi.org/10.3389/fphys.2014.00043

Wang, Li-Qiang; Zhao, Kun; Yuan, Han-Ye;, Wang, Qiang; Guan, Zeyuan; Tao, Jing; Li, Xiang-Ning; Sun, Yunpeng; Yi, Chuan-Wei; Chen, Jie; Li, Dan; Zhang, Delin; Yin, Ping; Liu, Cong; & Liang, Yi (2020). Cryo-EM structure of an amyloid fibril formed by full-length human prion protein. *Nature Structural & Molecular Biology, 27*(6), 598–602. https://doi.org/10.1038/s41594-020-0441-5

Watt, Nicole T.; & Hooper, Nigel M. (2003). The prion protein and neuronal zinc homeostasis. *Trends in Biochemical Sciences, 28*(8), 406–410. https://doi.org/10.1016/s0968-0004(03)00166-x

Westergard, Laura; Christensen, Heather M.; & Harris, David A. (2007). The cellular prion protein (PrPC): Its physiological function and role in disease. *Biochimica et Biophysica Acta (BBA) - Molecular Basis of Disease, 1772*(6), 629–644. https://doi.org/10.1016/j.bbadis.2007.02.011

Wille, Holger & Requena, Jesús. (2018). The Structure of PrPSc Prions. *Pathogens, 7*(1), 20. https://doi.org/10.3390/pathogens7010020

Zahn, Ralph; Liu, A., Lührs, T., Riek, R., Von Schroetter, C., López García, F., Billeter, M., Calzolai, L., Wider, G., & Wüthrich, K. (2000). NMR solution structure of the human prion protein. *Proceedings of the National Academy of Sciences, 97*(1), 145–150. https://doi.org/10.1073/pnas.97.1.145

Zhang, Yongbo; Swietnicki, Wieslaw; Zagorski, Michael G.; Surewicz, Witold K.; & Sönnichsen, Frank D. (2000). Solution Structure of the E200K Variant of Human Prion Protein. *Journal of Biological Chemistry, 275*(43), 33650–33654. https://doi.org/10.1074/jbc.C000483200